Nanoscale

Accepted Manuscript

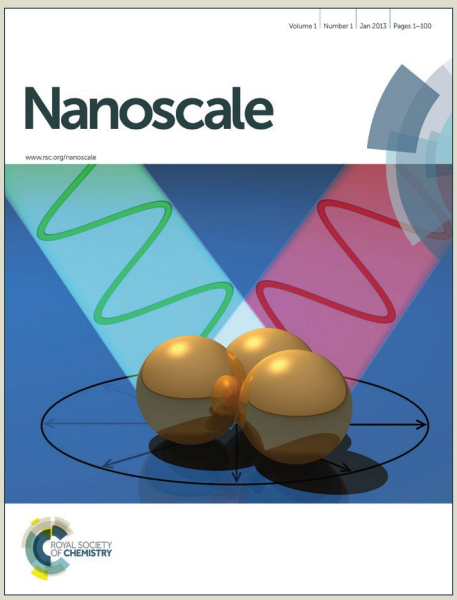

This is an *Accepted Manuscript*, which has been through the Royal Society of Chemistry peer review process and has been accepted for publication.

Accepted Manuscripts are published online shortly after acceptance, before technical editing, formatting and proof reading. Using this free service, authors can make their results available to the community, in citable form, before we publish the edited article. We will replace this *Accepted Manuscript* with the edited and formatted *Advance Article* as soon as it is available.

You can find more information about *Accepted Manuscripts* in the Information for Authors.

Please note that technical editing may introduce minor changes to the text and/or graphics, which may alter content. The journal's standard Terms & Conditions and the Ethical guidelines still apply. In no event shall the Royal Society of Chemistry be held responsible for any errors or omissions in this *Accepted Manuscript* or any consequences arising from the use of any information it contains.

ROYAL SOCIETY OF CHEMISTRY

www.rsc.org/nanoscale

Journal Name

RSCPublishing

ARTICLE

Phase-change materials filled hollow magnetic nanoparticles for cancer therapy and dual modal bioimaging†

Cite this: DOI: 10.1039/x0xx00000x

Received 00th January 2012,
Accepted 00th January 2012

DOI: 10.1039/x0xx00000x

www.rsc.org/

Jinghua Li, Yan Hu, Yanhua Hou, Xinkun Shen, Gaoqiang Xu, Liangliang Dai, Jun Zhou, Yun Liu and Kaiyong Cai*

To develop carriers for anti-cancer drug delivery, this study reports a biocompatible and thermal responsive controlled drug delivery system based on hollow magnetic nanoparticles (HMNP). The system is constructed simply by filling the hollow interiors of HMNP with phase-change material (PCM) of 1-tetradecanol that has a melting point of 38 ℃. The system achieves near "zero release" of both hydrophobic paclitaxel (PTX) and hydrophilic doxorubicin hydrochloride (DOX) and precise "on" or "off" drug delivery *in vitro* to efficiently induce cell apoptosis. Furthermore, the system displays both infrared thermal imaging and magnetic resonance imaging property. More importantly, the system demonstrates great potential for thermo-chemo combination cancer therapy *in vivo* when applying an alternating magnetic field.

1. Introduction

During the past decades, despite considerable progress had been achieved in medicine, cancer is still one of the leading causes to human death worldwide. [1] Low efficiency of currently available therapeutics hindered the healthcare of cancer patients. [2-4] Hyperthermia, heating body tissue globally or locally to kill tumor cells, is an efficient treatment for cancer therapy. [5, 6] By applying an alternating current magnetic field (AMF), magnetic materials could generate heat to destroy the tumor cells with no significant side and systematic effects. [7] Furthermore, the generated heat could boost immune response of the host and improve drug absorption by increasing the membrane fluidity. [3] When hyperthermia alone could not inhibit tumor efficiently, combined treatments with phototherapy, [8] radiotherapy, [9] chemotherapy *etc*.[10] could be considered. For instance, the combination of hyperthermia and chemotherapy, termed thermo-chemotherapy, has been proved to be an efficient approach for curing cancer. [11] Chemotherapy, the prevalent method for cancer therapy, however, have toxic side effect on normal body tissues and immune system. [12, 13]

To reduce the side toxicity of an anticancer drug and/or prolong the circulation time of the target drug, different controlled drug delivery systems were exploited. [14] Drug vehicles such as liposome, [15] gold nanoparticles, [16, 17] iron magnetic nanoparticles, [18] carbon nanoparticles, [19] mesoporous silica nanoparticles [20-22] and polymeric nanocomposites [23] had been extensively developed. Meanwhile, the clinical chemotherapy drugs are inherently either hydrophobic or hydrophilic. [24] Typically, hydrophobic drugs such as PTX are difficult to be delivered to blood plasma, while hydrophilic drugs such as DOX salt could not retain their long-term efficiency within body due to the tachytrophism. [25] It is thus urgent to design a universal drug delivery system for thermo-chemotherapy.

In this study, we designed and fabricated an AMF-triggered multifunctional controlled drug release system based on phase-change material (PCM) loaded HMNP for thermo-chemotherapy. PCM is one kind of material that has large latent heats of fusion, leading to melting and solidifying at a relatively constant temperature. [26] PCM could undergo three kinds of phase transitions: liquid-gas, solid-solid, and solid-liquid. Solid-liquid PCM was widely used both for fundamental research and practical application. In this study, we employed 1-tetradecanol as thermo-responsive PCM. The rationale was that 1-tetradecanol had good biocompatibility and exquisite critical solution temperature with melting point of around 38 ℃, [26] slightly higher than physiological temperature (37 ℃). Furthermore, the 1-tetradecanol has a hydrophilic head and a long hydrophobic tail, thus it could easily interact with either hydrophilic or hydrophobic chemical substances. [27] Anticancer drug of DOX was dissolved in PCM at a high temperature and then introduced into the interior of HMNP. Interestingly, the loading amount of DOX in HMNP@PCM could be precisely controlled simply by adjusting the ratio of drug to PCM. Meanwhile, since the PCM is in a solid state under physiological condition (37 ℃), the system could achieve "zero release" of drug for potential clinical application. It in turn eliminates the risk of drug toxicity before it reaches cancer lesion. Moreover, the DOX-loaded system could be targeted to tumor location by an external magnet. After endocytosis by tumor cells, the release of DOX associating with the melting PCM from HMNP@PCM@DOX could be triggered by an external AMF. Furthermore, the magnetic shell of the system could be utilized as T2 contrast agent for magnetic resonance imaging (MRI) and infrared (IR) thermal imaging to track tumor development after treatment. [28] We hypothesized that this system could load either hydrophilic or hydrophobic drug for controlled drug release *in vitro* and thermo-chemotherapy *in vivo* with dual-modality imaging potential.

Nanoscale Accepted Manuscript

2. Experimental

2.1. Materials

Styrene, methacrylic acid, Triton X-100 and Hoechst 33258 were supplied by Sigma Co. (St. Louis, MO, USA). 1-tetradecanol (PCM), rhodamine 6 G (R6G) and methylene blue (MB) were provided by Alfa Aesar Co (Tianjin, China). Potassium persulfate, potassium nitrate, potassium oxalate, paclitaxel (PTX), doxorubicin (DOX) were purchased from Aladdin Co. (Shanghai, China). Glycol, chloroform, sodium chloride were provided by Oriental Chemical Co. (Chongqing, China).

2.2. Materials fabrication

2.2.1. Preparation of hollow magnetic nanoparticles (HMNP). The HMNP was fabricated as follows: Firstly, we synthesized polystyrene (PS) nanoparticles as cores via a free-emulsion polymerization method. [29] Typically, 40 mL styrene, 10 mL methacrylic acid and 0.3 g potassium persulfate were dissolved into 500mL deionized water and added to a three-neck flask with ultra-sonification at room temperature for 10 min. The solution was purged with nitrogen before reaction to eliminate oxygen effects and heated to 72 ℃ with continuous stirring. The polymerization was continued for 24 h under nitrogen protection. Then the PS nanoparticles were collected by a centrifugal separation at 14000 rpm; Secondly, the core-shell nanoparticles PS@MNP were synthesized by controlling the hydrolysis of aqueous solutions of ferrous chloride and other divalent metal salts at the surface of PS nanoparticles. [30] Typically, 1 mL PS (5 wt %) colloid solution was dispersed into 200 mL distilled water under ultra-sonification for 5 minutes and then added to the metal salts solution containing 0.4 g $FeCl_3$ and 0.2 g $FeCl_2$, followed by adding 5.0 mL glycol for 10 min with ultrasonification. The mixture solution was incorporated with 2.5 g hexamethylene tetramine and 0.3 g potassium nitrate; then the solution was heated to 200 ℃ with continuous mechanical stirring for 3 h. The system was then cooled to room temperature. The core-shell magnetic nanoparticles were separated by an external magnet and washed with distilled water for 6 times and dried at 80 ℃ for 12 h; Finally, to produce hollow ferrite particles, the core-shell magnetic nanoparticles were calcined at 500 ℃ for 3 h under nitrogen-protection (heating rate: 10 ℃ min^{-1}). The obtained precipitate (noted as HMNP) was washed with distilled water for 6 times and then dried at 80 ℃.

2.2.2. Fabrication of drug delivery system. To obtain HMNP@PCM@DOX, the PCM was completely melted at 90 ℃ in a flask, various amounts of DOX was then added to the flask with continuous string for 2 h until the drug was entirely dissolved, [27] leading to different DOX concentrations (1.5, 3.0, 4.5, 6.0 and 7.5 μg/mL). The concentration of DOX, drug loading percentage (DL%) and drug loading efficiency (DLE %) were calculated as following equations:

$$C_{DOX} = \frac{m_{DOX}}{V + \frac{C_{HMNP@PCM@DOX} \times V \times 18.1\%}{0.824}}$$

$$\mathrm{DL}\ (\%) = \frac{\text{Weight of loaded DOX}}{\text{Total weight (HMNP+PCM+DOX)}} \times 100\%$$

$$\mathrm{DLE}\ (\%) = [1 - \frac{\text{Drug in supernatant liqiud}}{\text{Total drug added}}] \times 100\%$$

Where, C_{DOX} is the mass concentration of DOX; m_{DOX} is the mass of DOX; $C_{HMNP@PCM@DOX}$ is the mass concentration of HMNP@PCM@DOX; V means the solution volume to be used in experiments; the value of 18.1% is the loading weight percentage derived from thermal gravitational analysis (TGA) analysis; and the value of 0.824 is the density of PCM. Here, the volume contributions from HMNP and DOX were ignored since they were too trivial.

For instance, to obtain 1.5 μg/mL concentration of DOX in solution, supposing to use the concentration of HMNP@PCM@DOX as 0.25 mg/mL in experiments, 1.5 μg of DOX was dissolved into 43.75 μg of PCM and then dispersed with 0.21 mg of HMNP to fabricate HMNP@PCM@DOX. Then, 0.25 mg HMNP@PCM@DOX was dissolved into 1 mL PBS solution. To prepare other concentrations of HMNP@PCM@DOX, one needs to simply adjust the contents of DOX, PCM and HMNP. It should be pointed out that the drug loading percentage is highly dependent on the desired concentration of HMNP@PCM@DOX to be used.

Next, HMNPs were dispersed into the PCM/DOX mixture. Subsequently, chloroform was poured into the above mixture solution with continuous stirring and heating at 90 ℃ for 6 h. Along with the evaporation of chloroform, the PCM/DOX mixture permeated into the hollow cavity tardily through the small pores of HMNPs. Finally, excessive hot-water was added to the solution, resulting in two immiscible phases with obvious boundary, one is the HMNP encapsulated PCM/DOX mixture (noted as HMNP@PCM@DOX) in water phase, another is the unpackaged PCM/DOX in chloroform phase. The HMNP@PCM@DOX dispersing in water phase was collected by an external magnet. The HMNP@PCM and HMNP@PCM@PTX were prepared by similar procedures above.

2.3. Materials characterization

TEM images of the as-synthesized nanoparticles were obtained by using scanning electron microscopy (FEINova 400 Nano SEM, Philips, Netherlands). Thermal gravitational analysis (TGA) was performed with a thermal analyser (Micromeritics Co., USA) at 10 ℃ min-1 under Ar protection. The XRD patterns of different magnetic nanoparticles were recorded on an x-ray diffraction (Rigaku D/max 2500 PC, Japan). The magnetic property of different nanoparticles was characterized by vibrating sample magnetometer (VSM). The elemental analysis of particles was performed with an element analyser (Vario MAX CN, Germany). In vitro anticoagulation time evaluations were evaluated by using an automatic coagulation analyser (MC-2000, China). The surface charges of particles were measured by a potentiometric analyser (BIC, ZetaPALS, USA). The high frequency alternative magnetic field machinery was purchased from Shuangping Power Supply Technology Co. Ltd (Shenzhen, SP-04C, China).

2.4. Drug release

2.4.1. Dose-dependent thermogenesis. To verify the possibility of HMNP@PCM for magnetic hyperthermia, the calorigenic capability of magnetic nanoparticle was evaluated by using an AMF at a frequency of 200 KHz with voltage of 220 V. In the present study, we employed the solution of HMNP@PCM with different concentrations (0.5, 1.0, 1.5, 2.0 and 2.5 mg/mL), the temperature was measured every 5 min within 60 min.

Nanoscale Accepted Manuscript

This journal is © The Royal Society of Chemistry 2012

2.4.2. Temperature-dependent drug release. The PCM is in a solid state when the environmental temperature is lower than its melting point, while be in a liquid state when the temperature is above its melting point. Temperature is thus the most important factor to control drug release. To investigated the release behaviour of the magnetic drug carrier, HMNP@PCM@DOX (concentration: 2.0 mg/mL) in PBS solution was directly heated to various temperatures (20, 37, and 42 ℃) during 90 min period.

2.4.3. Time-dependent drug release. To investigate the encapsulation and release behaviour of the HMNP@PCM, two commonly used dyes with different solubility, *i.e.*, hydrophilic DOX) and hydrophobic PTX were chosen as model drugs. [24] We investigate the release behaviours of HMNP@PCM@DOX and HMNP@PCM@PTX for short-time (30 min) and long-time (15 days) with and without AMF (200 KHz, 300 A, 220 V).

2.5. *In vitro* study

2.5.1. Cell culture. Human hepatic carcinoma HepG2 cells were cultured with 1640 medium containing 10% fetal bovine serum (FBS, Gibco) at 37 ℃ under 5% CO_2 atmosphere with the adding of 100 U/mL of penicillin and 100 μg/mL streptomycin. The culture medium was changed every 2 days.

2.5.2 Cytotoxicity assay. The cytotoxicity of different nanoparticles was evaluated with MTT assay. HepG2 cells were seeded to 96-well plates at an initial cell density of 8×10^3 cells/cm^2. When cell confluence reached around 70-80%, the culture medium containing HMNP@PCM@DOX at different DOX concentrations (1.5, 3, 4.5, 6 and 7.5 μg/mL) was added to each well and incubated under AMF for 30 min. Then the HepG2 cells were cultured for another 6 h. After that, 2 mg/mL of MTT (50 μL) solution was added to each well and then incubated at 37 °C for another 3 h. Then, 150 μL DMSO was added to each well and incubated for another 10 min. Finally, the culture medium was collected in a 96-well plate and measured with a microplate reader (Bio-Rad 680, USA) at a wavelength of 570 nm.

2.5.3. Cell uptake assay. HepG2 cells were seeded to a 24-well plate at an initial cell density of 2×10^4 cells/cm^2. When cell confluence reached around 60-70%, the culture medium was replaced with fresh media containing HMNP@PCM at a concentration of 40 μg/mL. After incubation at 37 ℃ for 6 h and 12 h, the cells were digested by 0.25% trypsin-EDTA and washed by PBS. The cells were fixed by 2.5% glutaraldehyde for 24 h, after that the immobilized cells were sliced by paraffin section and then observed by TEM (TEM, H-600, Hitachi, Japan).

2.5.4. Cell apoptosis assay. To explore the apoptosis after thermo-chemo therapy, the subcellular localization of HMNP@PCM, free DOX and HMNP@PCM@DOX within HepG2 cells was investigated using confocal laser scanning microscopy (CLSM). Typically, HepG2 cells were cultured with PBS, HMNP@PCM, DOX, PTX, HMNP@PCM@DOX and HMNP@PCM@PTX. After treated with AMF for 30 min or without AMF, then the cells were incubated at 37 ℃ for another 6 h, the plate was washed with PBS for 3 times. The cells were then fixed by 2% paraformaldehyde at 4 ℃ for 25 min and washed with PBS for 3 times. Next, 0.2% Triton X-100 was added and kept at 4 ℃ for 2 min. Subsequently, cell nuclei were stained with Hoechst 33258 (10 μg/mL) for 3 min. Finally, the stained samples were mounted with 90% glycerinum. Cell nuclei were observed with a CLSM (LSM 710, Zeiss, Germany).

DNA fragmentation assay was also performed to investigate the apoptosis of HepG2 cells. DNA was extracted according to the operation manual of the cell apoptosis DNA ladder isolation kit, followed by identification via gel electrophoresis with 0.8% agarose gel.

2.5.5. Trypan blue staining assay. HepG2 cells were treated with thermo-chemotherapy for 30 min, and then stained by 0.4% trypan blue solution for 5 min, the trypan blue was washed out with PBS and recorded immediately using an optical microscope. [31]

2.6. *In vivo* study

2.6.1 Animal model. All animal experiments were performed according to the protocol approved by the Institutional Animal Care and Use Committee of China. Female nude mice of 4-6 weeks old with average weight of 20 g were purchased from Animal laboratory of Xinqiao Hospital (Chongqing). Nude mice were subcutaneously injected with 100 μL of a cell suspension containing 2×106 HepG2 cells. Typically, HepG2 tumor was bore at both groin sides of mice. We treated the right side of mice with different approaches, while the left side of mice was only treated with PBS. The tumor-bearing mice were divided into four groups (PBS, chemotherapy, hyperthermia and combined therapy groups, n=5 mice per group) followed by intratumorally administration of PBS, DOX, HMNP@PCM and HMNP@PCM@DOX at the right side of mice and then treated with AMF at the local tumor (once every other day, 30 minutes for each time). The injection dosage of DOX was around 10 μg (0.5 mg/kg) per mouse. 100 μL of PBS solution containing around 0.42 mg HMNP@PCM or HMNP@PCM@DOX was injected to each mouse. 10 μg of DOX was dissolved into 66 μg of PCM and then dispersed with 0.344 mg of HMNP to fabricate HMNP@PCM@DOX. The drug loading percentage was estimated as 2.38 % and the drug loading efficiency was about 97%.

2.6.2 Thermo-chemo combined therapy. When tumour volume reached about 50 mm^3, the tumor-bearing mice (n=5/group) were injected with PBS, HMNP, free DOX, HMNP@PCM@DOX at the right side of mice intratumorally and then treated with AMF at the local tumor (once every other day, 30 minutes for each time). The tumor sizes were measured with a caliper after post-injection every two days.

The tumor volume was calculated as $V_{tumour} = LW^2/2$ (L: the maximum length of tumor, W: the minimum width of tumor). The relative volume was defined as $(V\text{-}V_0)/V_0$ (V: current volume, V_0: initial tumor volume). [32] After feeding for 40 days, mortality rates were executed to further verify the biocompatibility and clinic effect.

2.6.3. Histological evaluation. To investigate the tissue responses to various treatments, the tumor-bearing mice were subjected to hyperthermia (HMNP@PCM with AMF), chemotherapy (DOX alone) and thermo-chemotherapy (HMNP@PCM@DOX with AMF). The tumors and major organs of the treated mice were taken out after intratumoral injection for 96 h, and fixed with formalin solution (10%) at 4 ℃ for 48 h. The tumors and organs were then embedded with paraffin and sliced for staining with hematoxylin-eosin (H&E). To evaluate the apoptosis in tumor tissue, tumor tissues stained with a TUNEL apoptosis detection kit (Beyontime, China). The nuclei of cells within tumor tissue were stained by Hoechst 33258 and observed with CLSM.

2.7. Dual modal imaging

2.7.1. Infrared thermal imaging. Infrared thermal imaging of HepG2 tumors bearing mice were treated with thermo-chemotherapy for 30 min and simultaneously recorded by an IR thermal camera (FLIRSystems Corporation, P20, USA).

Nanoscale Accepted Manuscript

2.7.2. MR imaging. Concentration-dependent T2-weighted MR images of HMNP@PCM@DOX nanocomposite were scanned under a 3 T clinical MRI scanner (Bruker Biospin Corporation, ClinScan, USA).[8] After the injection of HMNP@PCM@DOX, the T2-weighted MR images were procured during 30 min thermo-chemotherapy.

2.8. Statistical analysis

All data in this study were presented as means with standard deviation (SD). The statistical analysis was analysed by using software of OriginPro (version 7.5) via one-way analysis of variance (ANOVA) and Students's t-test. The confidence levels were set as 95% and 99%.

3. Results and discussion

3.1. Materials fabrication and characterization

The drug delivery system was fabricated as follows: firstly, polystyrene (PS) nanoparticles were synthesized to be used as cores; secondly, core-shell structures were obtained by coating ferrite shells onto the surfaces of the PS nanoparticles (PS@MNP); thirdly, the PS cores were calcined off at 500 ℃ to obtain the HMNP with internal cavities; Finally, drugs containing PCM were loaded into the cavities of HMNP by simple diffusion (HMNP@PCM@drug). Once triggering by an AMF, drug release from the system would induce cell apoptosis *in vitro* and thermo-chemotherapy *in vivo*. Meanwhile, the HMNP could be utilized as MR and/or IR imaging agent.

The morphologies of different nanoparticles were revealed by transmission electron microscopy (TEM). PS displayed well-distributed spherical structure with average diameter of around 134.7 ± 6.2 nm (**Fig. 1 A**, **a** & **Fig. S1 A**, **a**, Mean ± SD, n = 400). After coating with magnetic shell, PS@MNP nanocomposite displayed similar morphology to that of PS, while with increased average diameter of 165.1 ± 8.1 nm (**Fig. 1 A**, **b** & **Fig. S1 A**, **b**). After calcination, the obtained HMNP displayed discernible shell structure with shell thickness of about 15 nm (**Fig. 1 A c** & **Fig. S1 A**, **c**). After loading PCM, the as-synthesized HMNP@PCM remained similar round morphology and PCM was well defined in the hollow interior of HMNP (**Fig. 1 A**, **d**).

XRD patterns revealed that the as-synthesized HMNP was in a crystalline phase spine ferrite Fe_3O_4 (JCPDS card no. 85-1436) (**Fig. S1 B**). The magnetization values of PS@MNP, HMNP and HMNP@PCM were 22.6, 21.8 and 16.1emu/g, respectively. Such magnetization value of HMNP@PCM was high enough for magnetic targeting and hyperthermia application because it could rapidly respond to an external magnetic field (**Fig. 1 B**).

Moreover, we employed thermogravimetric analysis (TGA) to quantitatively characterize different samples. Around 18.1 wt% of PCM was encapsulated into the HMNP (**Fig. 1 C**), which was related to the much higher mass density of HMNP than that of PCM. Elemental analysis regarding the change of carbon content (**Table S1**) and zeta potentials measurements (**Table S2**) also proved that HMNP@PCM was successfully fabricated step by step.

To verify the feasibility of HMNP@PCM@DOX for magnetic hyperthermia application, the calorigenic potential of HMNP@PCM@DOX with different concentrations was characterized by using an AMF. The temperature rapidly reached the threshold temperature required for cancer hyperthermia (T>42 ℃) within 30 min by employing HMNP@PCM@DOX with concentration of 0.25 mg/mL (**Fig. S1 C**). The infrared thermographic maps also demonstrated that the HMNP@PCM@DOX had good thermogenesis when applying an AMF (**Fig. 1 D**).

Furthermore, to investigate the potential of HMNP@PCM@DOX to be as a T2 contrast agent for MR imaging. T2-weighted MR images of HMNP@PCM@DOX were recorded by a 3 T MR scanner. A concentration-dependent darkening effect was observed. Its transverse relaxivity (r_2) was about 92.7 $mM^{-1}s^{-1}$ (**Fig. 1 E**). It was attributed to the presence of the magnetic shell, which was consistent with a previous study. [8]

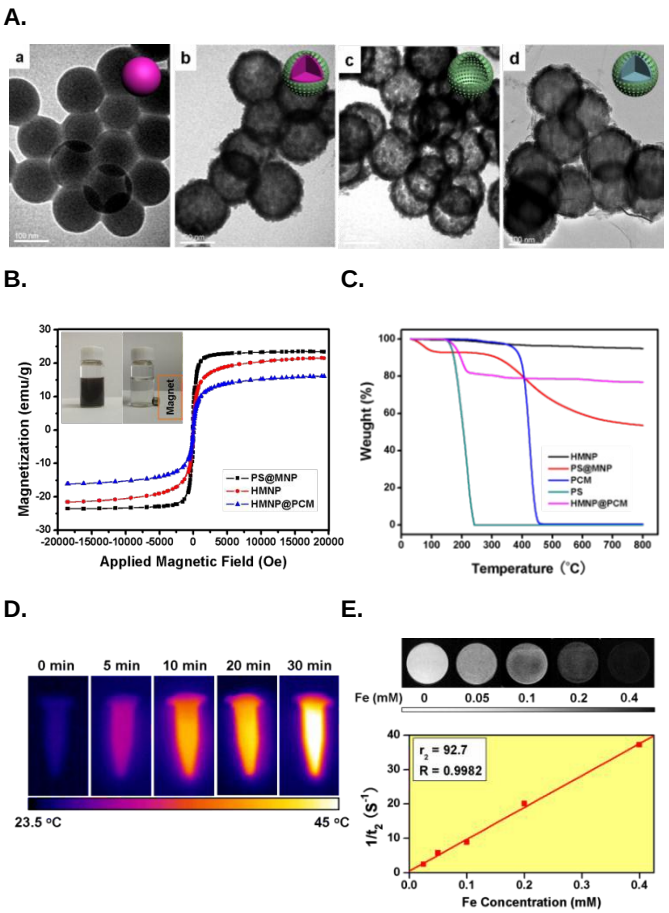

Figure 1. Physical property characterizations: **(A)** TEM images of different nanoparticles: **a**. PS nanoparticles; **b**. PS@MNP core-shell nanoparticles; **c**. HMNP nanoparticles; and **d**. HMNP@PCM nanoparticles, respectively; (**B**) Magnetic hysteresis loops of PS@MNP, HMNP and HMNP@PCM. Insert: photos of HMNP@PCM solution respond to a magnet field; (**C**) TGA curves of PS, PS@MNP, HMNP and MNP@PCM nanoparticles; (**D**) Infrared thermographic maps of centrifuge tubes containing HMNP@PCM@DOX solution triggered by an AMF (300 A, 200 kHz, 4 kW); and (**E**) Concentration-dependent T2-weighted MR images of HMNP@PCM@DOX nanocomposite.

3.2. Drug release

To investigate the release profile of HMNP@PCM system, both hydrophilic methylene blue (MB) and hydrophobic rhodamine 6G (R6G) were chosen as model drugs and quantified by UV-spectrophotometry. Structurally, a tetradecanol molecule has a hydrophilic head and a long hydrophobic tail, which makes it possible for encapsulating either hydrophilic or hydrophobic

Nanoscale Accepted Manuscript

This journal is © The Royal Society of Chemistry 2012

substances. [24] Both model drugs could be loaded and delivered by the system when applying an AMF (**Fig. 2 A**). Interestingly, we could achieve "on" or "off" pulsatile drugs release profiles for either hydrophilic or hydrophobic drugs (DOX or PTX) just simply switching on or off the applied AMF (300 A, 200 kHz, 4 kW) (**Fig. 2 B**). The pulsatile drug release behaviour of this system also has implication for other clinical application, such as diabetes treatment. [33] HMNP@PCM@DOX system displayed temperature-dependent drug release profile. Only negligible amount (4%) of DOX released from HMNP@PCM@DOX at physiological temperature, while around 80% of DOX released in 30 min corresponding to 42 ℃ (**Fig. 2 C**). Moreover, delayed drug release would be realized from HMNP@PCM@DOX system (**Fig. 2 D**), which again suggests the feasibility of AMF to be as the trigger for controlled drug release. The underlying mechanism was that the high-frequency AMF led to the temperature of HMNP@PCM@drug system increased above the melting point of PCM, leading to drugs release; on the other hand, once switching off the AMF, the system temperature dropped down below the melting point of PCM, resulting in PCM changed from liquid phase to solid phase to end up the drug release.

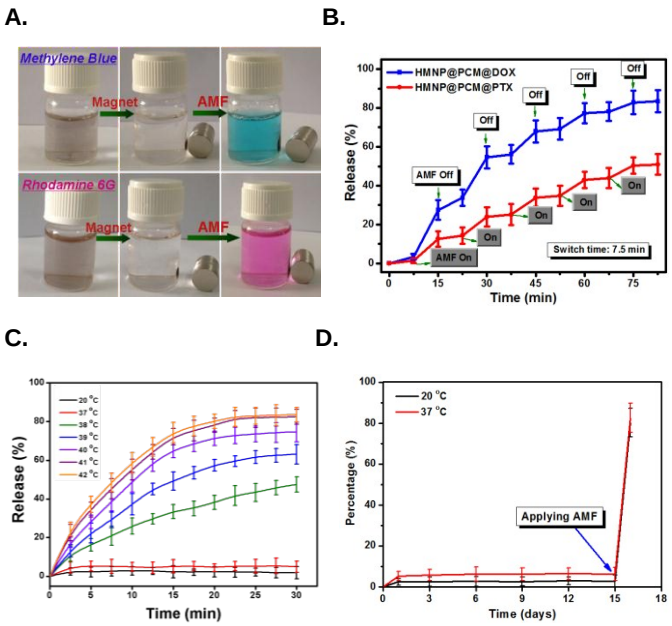

Figure 2. (**A**) Photographs of HMNP@PCM@MB and HMNP@PCM@R6G solution before and after heating by an AMF; (**B**) The on-off switch of drug release profiles of HMNP@PCM@DOX and HMNP@PCM@PTX in presence of AMF; (**C**) Temperature-responsive release profiles of HMNP@PCM@DOX; and (**D**) Delayed drug release of HMNP@PCM@DOX at different temperatures and then treated with an AMF (300 A, 200 kHz, 4 kW, 30 min).

3.3. *In vitro* assays

3.3.1. Cytotoxicity evaluation

To quantitatively evaluate the cytotoxicity of HMNP@PCM@DOX and HMNP@PCM@PTX, as well as their therapeutic sensitivities to AMF, we performed dose-dependent cytotoxicity assay. Both HMNP@PCM@DOX and HMNP@PCM@PTX systems displayed desirable thermotherapy potential. Moreover, these systems without AMF treatment displayed similar cell viability to that of control, suggesting their good biocompatibility. A previous study also confirmed that tetradecanol had good biocompatibility and low toxicity (oral, rat LD50>5 g/kg) for potential clinical application. [24] As for AFM treatment, the results suggest that higher DOX or PTX loading amount led to higher cytotoxicity (**Fig. 3 A** & **B**). It was related to the fact that either DOX or PTX released from the system when treated with AMF. HMNP@PCM@DOX displayed higher cell growth inhibition effect than that of HMNP@PCM@PTX. The phenomenon could be explained that the hydrophilic DOX salt (versus hydrophobic PTX) was water soluble, leading to high cell uptake and cell death. Trypan blue staining assay also revealed that HMNP@PCM@DOX nanoparticles could efficiently induce cell death (blue cells), however, only when they exposed to an external AMF (**Fig. S2 A**). Moreover, along with increasing exposure time, more dead cells were observed (**Fig. S2 B**).

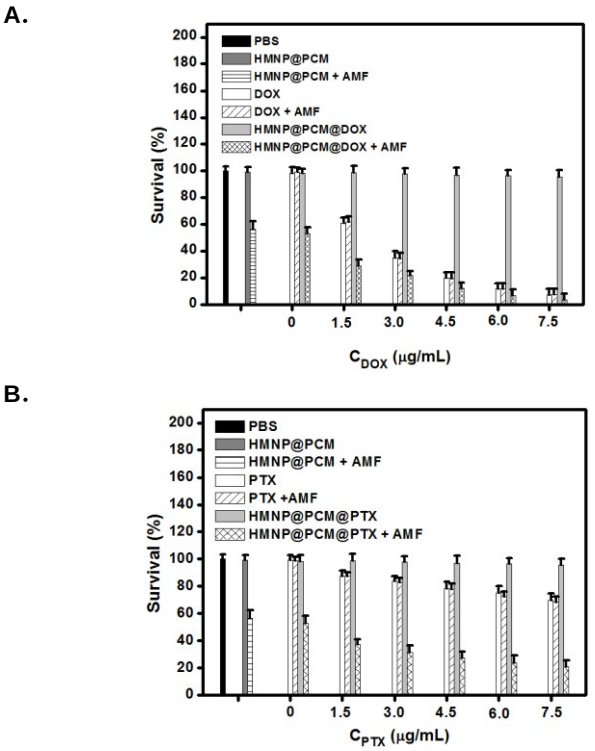

Figure 3. Dose-dependent cytotoxicity assays: HepG2 cells treated with (**A**) HMNP@PCM@DOX and (**B**) HMNP@PCM@PTX in presence or absence of AMF (300 A, 200 kHz, 4 kW, 30 min).

3.3.2. Cell uptake and distribution

To investigate the interaction between HMNP@PCM@DOX and HepaG2 cells, we employed confocal laser scanning microscopy (CLSM) and TEM to observe the cell morphologies. After incubation for 12 h, negligible cell death was observed in the PBS, HMNP@PCM and HMNP@PCM@DOX without AMF treatment, indicating that the system had good biocompatibility. However, the thermo-chemo combined therapy group (HMNP@PCM@DOX with AMF) presented much better cell death compared with those of hyperthermia (HMNP@PCM with AMF) or chemotherapy (DOX alone) treatment (**Fig. 4 A**). Transmission electron microscopy (TEM) observation revealed that HMNP@PCM@DOX nanoparticles mostly distributed at cytoplasm, while not entering cells nuclei (**Fig. S3**).

3.3.3. DNA-ladder assay

To investigate the potential curative mechanism of the systems, we performed DNA fragmentation assay. Both HMNP@PCM@DOX and HMNP@PCM@PTX treated with AMF

Nanoscale Accepted Manuscript

displayed higher intensity of DNA fragmentation than those of other groups. The potential mechanism lies in that HMNP@PCM@drug system could efficiently deliver either hydrophilic or hydrophobic drug to cells' cytoplasm and in turn led to apoptosis (**Fig. 4 B**).

A.

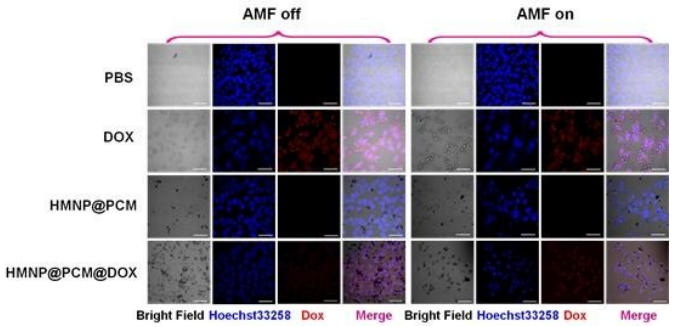

B.

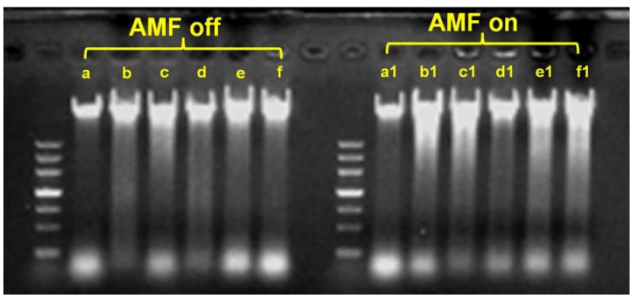

Figure 4. CLSM images (**A**) and DNA fragmentation assay (**B**) of HepG2 cells co-cultured with different samples in presence or absence of AMF treatment (300 A, 200 kHz, 4 kW, 30 min). Red: DOX, blue: cell nuclei. Scale bar: 50 μm. PBS: **a** & **a1**; HMNP@PCM: **b** & **b1**; DOX: **c** & **c1**; PTX: **d** & **d1**; HMNP@PCM@DOX: **e** & **e1**; and HMNP@PCM@PTX: **f** & **f1**. The concentration of HMNP@PCM@DOX or HMNP@PCM@PTX was 0.25 mg/mL with equivalent DOX or PTX concentration of 6.0 μg/mL.

3.4. *In vivo* evaluations

To investigate the thermal-chemo therapy and feasibility of HMNP@PCM@DOX for potential clinic application, we performed detailed *in vivo* evaluations. Compared with single therapeutic treatment, thermal-chemo combination therapy led to nearly complete remission of liver tumors was noted after 16 days' therapy (**Fig. 5 A**). Relative tumor volumes proved the synergetic cancer therapeutic effects of thermo-chemo combined therapy (**Fig. 5 B**). The chemotherapy group with free DOX showed worse curative effect, mainly due to its short blood circulation time. Since the 8th day's treatment, the relative tumor volume thermo-chemo combination therapy group was significantly lower ($p<0.01$) than those of other groups. Moreover, the survival rate of combined therapy group was much higher (100%) than DOX-chemotherapy (40%) alone (**Fig. 5 C**), indicating its advantage regarding toxic side effects over conventional chemotherapy.

To investigate the potential mechanism of thermo-chemo combined therapy *in vivo*, we performed tissue TUNEL staining assay. The result shows that HMNP@PCM@DOX system with AMF treatment led to severe cell apoptosis within tumor tissue, [31] which was revealed by the large amount apoptotic DNA fragments (pink dots) (**Fig. 5 D**). It thus contributed to the tumor growth inhibition. Furthermore, a time-dependent cell apoptosis was observed in tumor tissue (**Fig. S4**).

To investigate the potential toxic side effect of the system, we further performed histopathological examination on the major organs (tumor, heart, lung, kidney, liver and spleen) of mice after thermo-chemotherapy with hematoxylin-eosins (H&E) staining (**Fig. 5 E**). The tumors treated with thermo-chemo combined therapy displayed much severe damage. As for the organs of liver, spleen, lung and kidney, no obvious damage was observed in each group.

A.

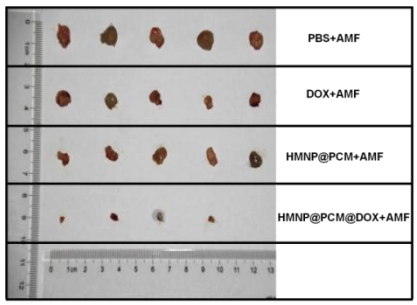

B.

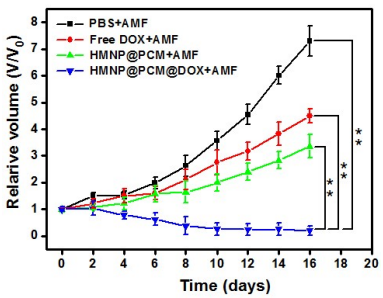

C.

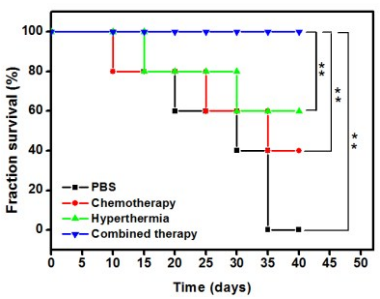

D.

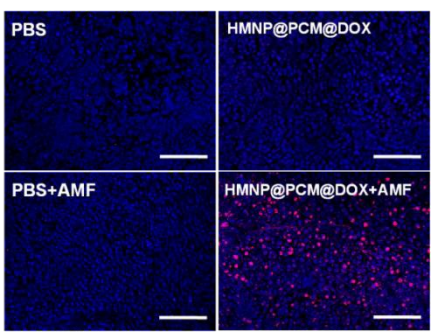

Nanoscale Accepted Manuscript

This journal is © The Royal Society of Chemistry 2012

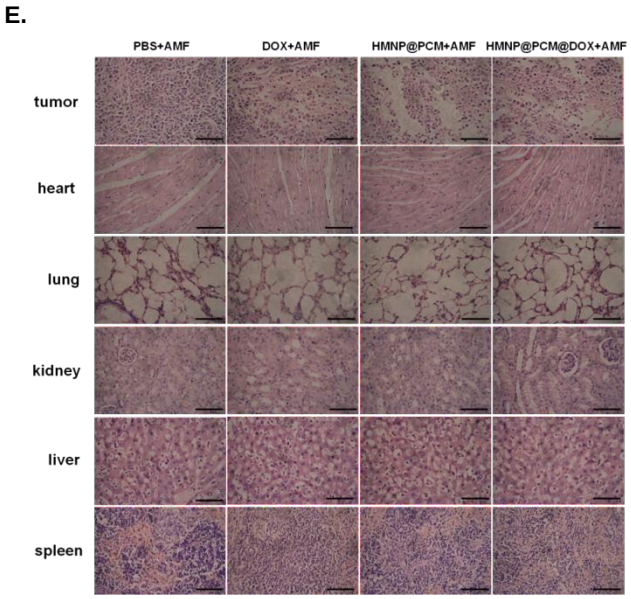

Figure 5. *In vivo* evaluations of thermo-chemo combination cancer therapy: (**A**) Photographs of the tumors at the end of treatments; (**B**) Tumor growth curves of different groups after various treatments; (**C**) Survival rates of tumors bearing mice with different treatments, $p<0.01$; (**D**) Apoptosis assay of tumor tissues with TUNEL method. Pink: apoptosis DNA; blue: cell nuclei; and (**E**) Histological evaluations of major organs (tumor, heart, lung, kidney, liver and spleen) of mice with H & E staining. Scale bar: 100 μm.

3.5. Dual modal imaging

With the advancement of nanomedicine, multifunctional magnetic nanoparticles provide great convenience for imaging-guided cancer therapy. [28, 34-37] To investigate the dual modal imaging potential of the system, we firstly employed an IR thermal camera to monitor the temperature change of mice during AMF loading (**Fig. 6 A**). Mice treated with HMNP@PCM@DOX showed obvious heat production at tumor region. The temperature increased to around 44 ℃ in 30 min, whereas the surrounding tissue near the tumor showed only a moderate temperature (35-37 ℃). In contrast, the tumor temperature of mice injected with PBS exhibited no significant increase (below 35 ℃) during 30 min of AMF loading (**Fig. 6 B**).

We also obtained the MR images at day 0 and day 7. After injection with HMNP@PCM@DOX, the acquired T2-weighted MR images showed strong darkening effect at the tumor area (**Fig. 6 C**, arrows), which provided further proof for tumor growth inhibition after combined therapy by HMNP@PCM@DOX nanocomposite. All results confirm the feasibility of HMNP@PCM@DOX system for image-guided cancer therapy.

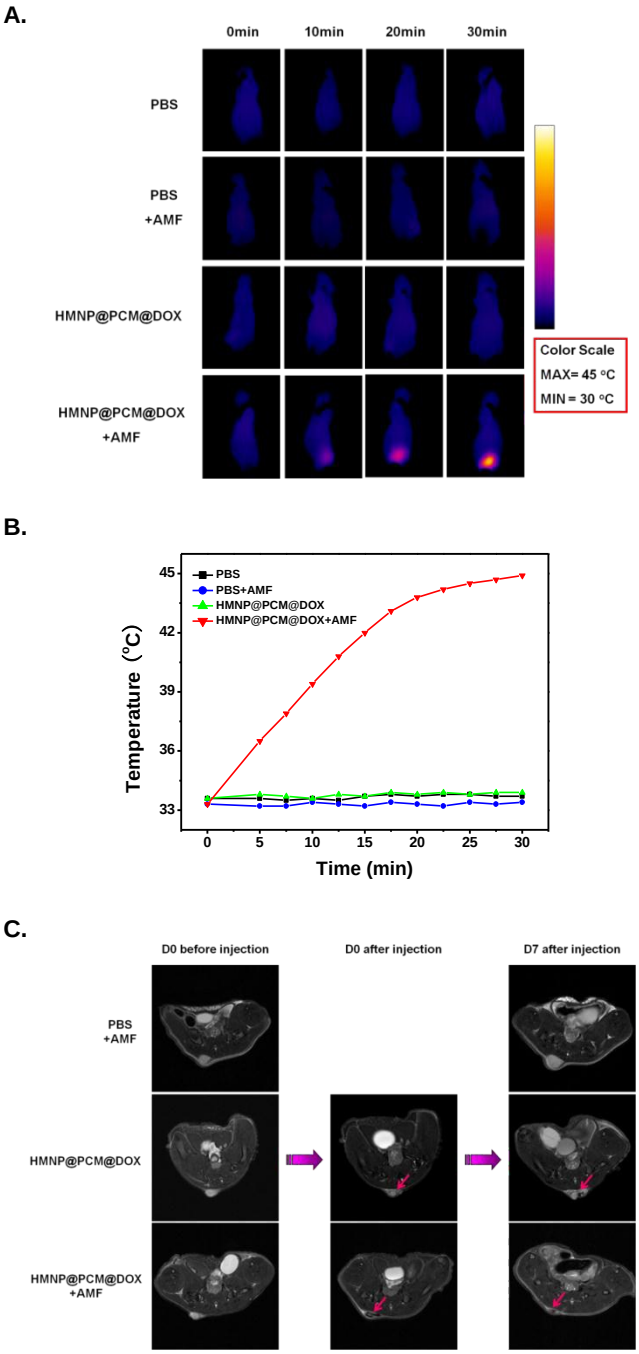

Figure 6. Bioimaging characterization: (**A**) Infrared thermographic images of tumor-bearing nude mice subjected to thermo-chemo combination cancer therapy; (**B**) Tumor temperatures change with different treatments recorded by IR thermal camera; and (**C**) Representative MR images of nude mice from three different groups obtained at day 0 before and after injection and day 7 after treatment.

Taken together, we confirmed our hypothesis that HMNP@PCM system could deliver either hydrophilic or hydrophobic drug in a controlled manner in vitro and multimodal image-guided thermo-chemotherapy in vivo. The designed system of HMNP@PCM has potential advantages as follows: First, a near "zero release" behaviour was realized at physiological temperature (37 ℃), since the melting point of PCM (38 ℃) is higher than that of the former one, which could heavily reduce the drug toxicity before

Nanoscale Accepted Manuscript

it reaches tumor site; Second, the loading dose of anticancer drug into HMNP could be precisely controlled simply by adjusting the proportion of drug to PCM; Third one, the tumor could be easily treated with an external AMF to trigger the drug release and to simultaneously start hyperemia.

4. Conclusion

In summary, we report an alternative to develop multifunctional nanocarrier that could load either hydrophobic or hydrophilic drugs based on HMNP for imaging-guided thermo-chemo combination cancer therapy. The system demonstrated sensitive thermal response to AMF for triggering switchable controlled drug delivery with nearly "zero release" feature. More importantly, the system showed good anti-tumor efficiency, while with minimal toxic side effect. The study provides a platform for the fabrication of new generation nanocarrier for efficient cancer therapy.

Acknowledgements

We gratefully acknowledge the financial support from Natural Science Foundation of Chongqing Municipal Government (CSTC2013kjrc-ljrcpy0004), National Natural Science Foundation of China (21274169 and 31170923), National Key Technology R&D Program of the Ministry of Science and Technology (2012BAI18B04) and Fundamental Research Funds for the Central Universities (CQDXWL-2013-Z002).

Notes and references

Key Laboratory of Biorheological Science and Technology, Ministry of Education, College of Bioengineering, Chongqing University, Chongqing 400044, PR China. Fax: (+) 86-23-65112619 ; Tel:(+) 86-23-65112619; E-mail: kaiyong_cai@cqu.edu.cn

† Electronic Supplementary Information (ESI) available: [TEM images and particle size distribution, XRD patterns of different nanoparticles, Trypan blue staining, Cell uptake (TEM imges), TUNEL staining, Elemental analysis, Zeta-potential measurements].

1 A. Jemal, F. Bray, M. Center, J. Ferlay, E. Ward and D. Forman, *CA Cancer J. Clin.,* 2011, **61**, 69-90.
2 R. Petros and J. DeSimone, *Nat. Rev.,* 2010, **9**, 615-628.
3 S. Chandra, K. Barick and D. Bahadur, *Adv. Drug Deliv. Rev*., 2011, **63**, 1267-1281.
4 Z. Zhang, J. Wang and C. Chen, *Adv. Mater.,* 2013, **25**, 3869-3880.
5 Z. Luo, X. Ding, Y. Hu, S. Wu, Y. Xiang, Y. Zeng, B. Zhang, H. Yan, H. Zhang, L. Zhu, J. Liu, J. Li, K. Y. Cai and Y. L. Zhao, *ACS Nano,* 2013, **7**, 10271-10284.
6 Z. Chen, Z. Li, J. Wang, E. Ju, L. Zhou, J. Ren and X. Qu, *Adv. Funct. Mater*., 2014, **24**, 522-529.
7 C. Fang, F. M. Kievit, O. Veiseh, Z. R. Stephen, T. Wang, D. H. Lee, R. G. Ellenbogen and M. Zhang, *J. Control. Release,* 2012, **162**, 233-241.
8 C. Wang, H. Xu, C. Liang, Y. Liu, Z. Li, G. Yang, L. Cheng, Y. Li and Z. Liu, *ACS Nano,* 2014, **7**, 6782-6795.
9 W. Fan, B. Shen, W. Bu, F. Chen, K. Zhao, S. Zhang, L. P. Zhou, W. Peng, Q. Xiao, H. Xing, J. Liu, D. Ni, Q. He and J. Shi, *J. Am. Chem. Soc.,* 2013, **135**, 6494-6503.
10 I. I. Slowing, J. L. Vivero-Escoto, C.W. Wu and V. S. Lin, *Adv. Drug. Deliv. Rev.,* 2008, **60**, 1278-1288.
11 J. L. Markman, A. Rekechenetskiy, E. Holler and J.Y. Ljubimova, *Adv. Drug Deliv Rev.,* 2013, **65**, 1866-1879.
12 S. MacEwan and A. Chilkoti, *Nano lett*., 2012, **12**, 3322-3328.
13 X. Ma, Y. L. Zhao and X. J. Liang, *Acc. Chem. Res.,* 2011, **44**, 1114-1122.
14 J. Wang , X. Sun, W. Mao, W. Sun, J. Tang, M. Sui, Y. Shen and Z. Gu, *Adv. Mater.,* 2013, **25**, 3670-3676.
15 X. Ding, K. Cai, Z. Luo, J. Li, Y. Hu and X. Shen, *Nanoscale,* 2012, **4**, 6289-6292.
16 J. Lu, M. Liong, Z. Li, J.I. Zink and F. Tamanoi, *Small*, 2010, **6**, 1794-1805.
17 J. Song, J. Zhou and H. Duan, *J. Am. Chem. Soc.*, 2012, **134**, 13458-13469.
18 Z. Luo, K. Cai, Y. Hu, J. Li, X. Ding, B. Zhang, D. Xu, W. Yang and P. Liu, *Adv. Mater*., 2012, **24**, 431-435.
19 S. Boncel, P. Zając and K. K.K. Koziol, *J. Control. Release*, 2013, **169**, 126-140.
20 X. Yang, Z. Li, M. Li, J. Ren and X. Qu, *Chem.-Eur. J.*, 2013, **19**, 15378-15383.
21 Y. Hu Y, K. Y. Cai, Z. Luo and K. D. Jandt, *Adv. Mater.,* 2010, **22**, 4146-4150.
22 X. Ma, K. Nguyen, P. Borah, C. Ang and Y. Zhao, *Adv. Healthcare Mater*., 2012**, 1**, 690-697.
23 J. Xu, F. Gattacceca and M. Amiji, *Mol. Pharm.,* 2013, **10**, 2031-2044.
24 G. Moon, S. Choi, X. Cai, W. Li, E. Cho, U. Jeong, L. Wang and Y. Xia, *J. Am. Chem. Soc.,* 2011, **133**, 4762-4765.
25 S. Egli, M. G. Nussbaumer, V. Balasubramanian, M. Chami, N. Bruns, C. Palivan and W. Meier, *J. Am. Chem. Soc.,* 2011, **133**, 4476-4483.
26 D. C. Hyun, N. S. Levinson, U. Jeong and Y. Xia, *Angew. Chem. Int. Ed.,* 2014, **53**, 3780-3795.
27 L. Tian, N. Gandra and S. Singamaneni, *ACS Nano,* 2013, **7**, 4252-4260.
28 X. Song, H. Gong, S. Yin, L. Cheng, C. Wang, Z. Li, Y. Li, X. Wang, G. Liu and Z. Liu, *Adv. Funct. Mater*., 2014, **24**, 1194-1201.
29 Y. Zhang, Z. Huang, F. Tang and J. Ren, *Thin Solid Films,* 2006, **515**, 2555-2561.
30 L. Xia, M. Zhang, C. Yuan and M. Rong, *J. Mater. Chem.,* 2011, **21**, 9020-9026.
31 B. L. Zhang, Z. Luo, J. J. Liu, X. W. Ding, J. H. Li and K.Y. Cai, *J. Control. Release*, 2014, **192**, 192-201.
32 M. M. Tomayko and C. P. Reynolds, *Cancer Chemoth. Pharm.,* 1989, **24**, 148-154.
33 K. Y. Cai, Z. Luo, Y. Hu, X. Y. Chen, L. Yang and L. H. Deng, *Adv. Mater*., 2009, **21**, 4045-4049.
34 Y. Huang, S. He, W. Cao, K. Cai and X. Liang, *Nanoscale,* 2012, **4**, 6135-6149.
35 J. Li, L. Zheng, H. Cai, W. Sun, M. Shen, G. Zhang and X. Shi, *Biomaterials*, 2013, **34**, 8382-8392.
36 J. Li, Y. He, W. Sun, Y. Luo, H. Cai, Y. Pan, M. Shen, J. Xia and X. Shi, *Biomaterials*, 2014, **35**, 3666-3677.
37 J. Li, Y. Hu, J. Yang, P. Wei, W. Sun, M. Shen, G. Zhang and X. Shi, *Biomaterials*, 2015, **38**, 10-21.

Nanoscale Accepted Manuscript

 This journal is © The Royal Society of Chemistry 2012

Entry for the Table of Contents

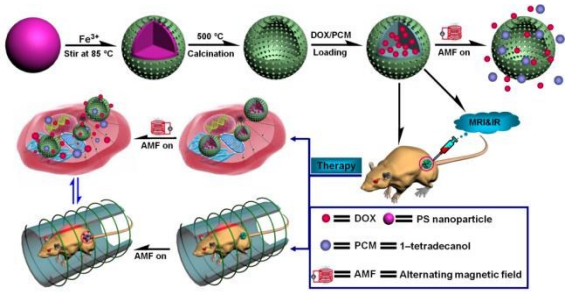

An alternating magnetic field triggered nanocarrier for drug delivery is fabricated for dual modal imaging-guided thermo-chemo cancer therapy.

Nanoscale Accepted Manuscript